Simple binding of protein kinase A prior to phosphorylation allows CFTR anion channels to be opened by nucleotides

Csaba Mihályi[a,b,c], Iordan Iordanov[a,b,c], Beáta Töröcsik[a,b,c], and László Csanády[a,b,c,1]

[a]Department of Medical Biochemistry, Semmelweis University, H-1094 Budapest, Hungary; [b]Magyar Tudományos Akadémia - Semmelweis Egyetem (MTA-SE) Ion Channel Research Group, Semmelweis University, H-1094 Budapest, Hungary; and [c]Hungarian Center of Excellence for Molecular Medicine - Semmelweis Egyetem (HCEMM-SE) Molecular Channelopathies Research Group, Semmelweis University, H-1094 Budapest, Hungary

Edited by Richard W. Aldrich, The University of Texas at Austin, Austin, TX, and approved July 27, 2020 (received for review April 24, 2020)

The Cystic Fibrosis Transmembrane Conductance Regulator (CFTR) anion channel is essential for epithelial salt–water balance. CFTR mutations cause cystic fibrosis, a lethal incurable disease. In cells CFTR is activated through the cAMP signaling pathway, overstimulation of which during cholera leads to CFTR-mediated intestinal salt–water loss. Channel activation is achieved by phosphorylation of its regulatory (R) domain by cAMP-dependent protein kinase catalytic subunit (PKA). Here we show using two independent approaches—an ATP analog that can drive CFTR channel gating but is unsuitable for phosphotransfer by PKA, and CFTR mutants lacking phosphorylatable serines—that PKA efficiently opens CFTR channels through simple binding, under conditions that preclude phosphorylation. Unlike when phosphorylation happens, CFTR activation by PKA binding is completely reversible. Thus, PKA binding promotes release of the unphosphorylated R domain from its inhibitory position, causing full channel activation, whereas phosphorylation serves only to maintain channel activity beyond termination of the PKA signal. The results suggest two levels of CFTR regulation in cells: irreversible through phosphorylation, and reversible through R-domain binding to PKA—and possibly also to other members of a large network of proteins known to interact with the channel.

ABC protein | protein kinase A | consensus serine | intrinsically disordered | N^6-(2-phenylethyl)-ATP

Cystic Fibrosis Transmembrane Conductance Regulator (CFTR) is an anion-selective channel (1, 2) expressed at the apical surface of epithelial cells lining the lung, intestine, the pancreatic duct, and the sweat duct. CFTR-mediated anion transport is indispensable for the salt–water homeostasis of these tissues. Loss-of-function mutations in CFTR cause cystic fibrosis, a devastating incurable multiorgan disease (3). In epithelial cells CFTR channels are activated by signals that elevate cytosolic cAMP levels, causing dissociation of the regulatory and catalytic subunits of cAMP-dependent protein kinase which colocalizes with CFTR (4, 5). The released catalytic subunit (PKA) activates CFTR by phosphorylating it at multiple (~11) target serines located mostly in its cytosolic regulatory (R) domain (6–9). During secretory diarrheas, like cholera, bacterial toxins irreversibly activate adenylate cyclase, causing a persistent increase in cAMP levels in the intestinal epithelium. The ensuing persistent PKA activity keeps CFTR channels permanently open, resulting in precipitous salt–water loss into the lumen of the gut (10).

CFTR belongs to the family of ATP Binding Cassette (ABC) proteins and contains two transmembrane domains (TMDs) that form the channel pore, each followed by a cytosolic nucleotide binding domain (NBD). These two ABC-canonical TMD–NBD halves are linked by the unique cytosolic R domain, which shows no sequence homology to any known protein (1), and forms an intrinsically disordered peptide segment (11).

Phosphorylated CFTR channels are gated by ATP through a mechanism that is based on conformational changes conserved among ABC proteins. Upon ATP binding the two NBDs dimerize, and this process is coupled to pore opening. Upon ATP hydrolysis the NBD dimer dissociates and the pore closes (12). The closed CFTR pore resembles the inward-facing, the open pore the outward-facing, TMD conformation of related ABC proteins (13–16).

In contrast to the ATP-dependent gating cycle, the mechanism of CFTR regulation by R-domain phosphorylation is poorly understood. The unphosphorylated R domain must inhibit channel gating, because its deletion results in CFTR channels that can open in the presence of ATP without prior phosphorylation (17, 18). But, how phosphorylation leads to channel activation has remained unclear. In electron cryomicroscopy structures of unphosphorylated apo CFTR a density for the R domain is seen wedged in between the NBDs and the cytosolic ends of the TMD helices, preventing NBD dimerization and flipping of the TMDs into the outward-facing, open conformation (13, 14). Correspondingly, in structures of phosphorylated, outward-facing CFTR no density for the R domain is observed, suggesting that upon phosphorylation it becomes entirely disordered and released from its occluded position (15, 16). As it is unclear how PKA might have access to the occluded R domain, it was suggested that phosphorylation might follow infrequent

Significance

Ion channels are protein pores that pass ions across biological membranes. CFTR is an anion channel required for proper salt–water transport across epithelia, including the lung and the gut. CFTR overactivation due to bacterial toxins causes severe diarrhea (e.g., in cholera), and impaired activation due to mutations underlies cystic fibrosis, a lethal disease. CFTR is activated by a kinase (PKA) which phosphorylates the channel. Here we show that CFTR activation is not caused by phosphorylation, as believed, but by simple PKA binding which promotes reversible release of CFTR's regulatory (R) domain from an inhibitory position. Subsequent R-domain phosphorylation renders activation irreversible. Reversible channel activation is likely mediated by several members of a large protein network that interacts with CFTR.

Author contributions: C.M., I.I., and L.C. designed research; C.M. and I.I. performed research; B.T. and L.C. contributed new reagents/analytic tools; C.M., I.I., and L.C. analyzed data; and C.M., I.I., and L.C. wrote the paper.

The authors declare no competing interest.

This article is a PNAS Direct Submission.

[1]To whom correspondence may be addressed. Email: csanady.laszlo@med.semmelweis-univ.hu.

This article contains supporting information online at https://www.pnas.org/lookup/suppl/doi:10.1073/pnas.2007910117/-/DCSupplemental.

First published August 17, 2020.

spontaneous R domain release, resulting in a two-step activation process (Fig. 1*B*) in which channels sequentially transition from a "wedged-in" inactive (W), through a "released" marginally active (R), to the "phosphorylated" fully active (P) state—consistent with the sigmoidal shape of macroscopic CFTR current activation time courses in inside out patches exposed to PKA (Fig. 1*A*, red curve) (14). Rapid partial current deactivation observed within seconds of PKA removal (Fig. 1 *A*, *Right*; see blue curve) was suggested to reflect rapid partial dephosphorylation (to state D; Fig. 1*B*), leaving channels with a lower open probability (P_o) (14, 18). Here we set out to test the validity of this generally accepted mechanistic model through a series of experiments specifically designed to allow distinction of effects caused by PKA binding versus phosphorylation. The results fundamentally reshape our understanding of the mechanism by which PKA regulates CFTR channel activity.

Results

PKA Dependence of CFTR Current Activation Hints at Possibly Distinct Effects of PKA Binding and Phosphorylation. To examine how current activation depends on the concentration of applied PKA, inside out patches containing wild-type (WT) CFTR channels were exposed to various test PKA concentrations (Fig. 2). After the currents had settled in the test [PKA] (Fig. 2, segment *a*), maximal (300 nM) PKA was briefly applied to fully phosphorylate the channels, allowing normalization of the currents, obtained from different patches, to their maximal values (segment *b*). [PKA] was then returned to its test value (segment *c*), and finally the kinase was removed (segment *d*). Interestingly, already at low PKA concentrations, such as 33 nM (Fig. 2, blue trace), currents before exposure to maximal [PKA] (segment *a*) approached those after exposure to maximal [PKA] (segment *c*) (see Fig. 2, *Inset*, dark blue symbols). This observed pattern of

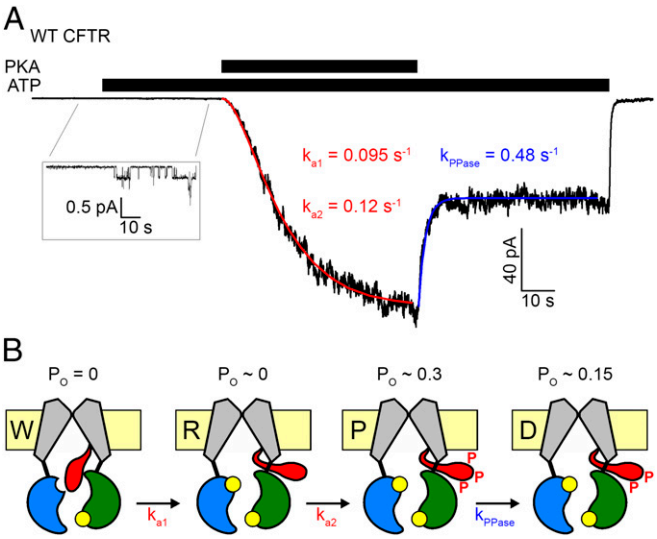

Fig. 1. Prevailing mechanistic interpretation of CFTR activation by PKA. (*A*) Sigmoidal activation time course of macroscopic CFTR current in an inside out patch exposed to 2 mM ATP plus 300 nM PKA (black bars), and rapid partial deactivation upon PKA removal. Red and blue curves are fits to the two-step activation and the single-step partial deactivation process, respectively, depicted in *B*, with fitted rate constants plotted. (*B*) Cartoon interpretation of the data in *A*, by assuming sequential shuttling through channel states W (wedged in, P_o = 0), R (released, P_o vanishingly small; compare *A*, *Inset*) and P (phosphorylated, P_o~0.3) during activation, and from P to D (partially dephosphorylated, P_o~0.15) upon PKA removal. TMDs, gray; NBD1, blue; NBD2, green; R domain, red; ATP, yellow.

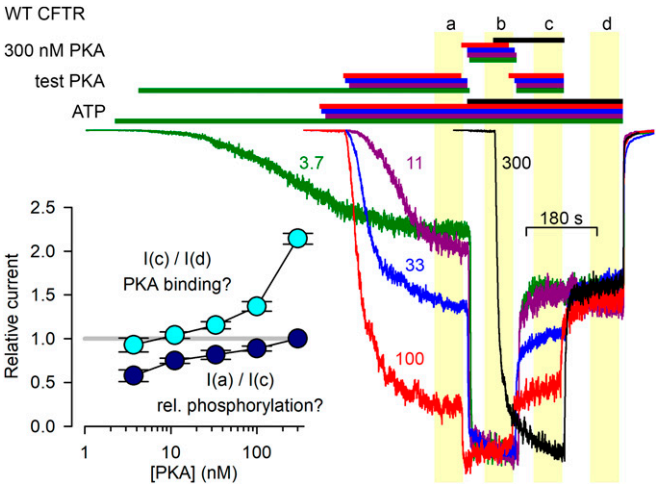

Fig. 2. PKA-dependent CFTR current activation/deactivation time courses hint at the possibility of CFTR activation by PKA binding. Macroscopic CFTR currents from patches exposed, in sequential order, to test [PKA], 300 nM PKA, test [PKA], and 0 nM PKA, all in 2 mM ATP. Current traces and bars that identify exposure to compounds are color coded based on the value of the test [PKA] which is indicated (in nM) next to each trace. Final steady-state stretches of the four experimental segments are highlighted by yellow boxes and marked *a* through *d*. Currents were normalized to their average values in segment *b*, and are shown synchronized to the end of segment *d*. (*Inset*) Current-amplitude ratios [mean± SEM (n = 7–38)] between indicated experimental segments as a function of test [PKA].

[PKA] dependence of current activation/deactivation time courses affords two possible explanations.

Based on the prevailing interpretation (Fig. 1*B*), at low [PKA] only low phosphorylation stoichiometries are achieved, due to strong endogenous membrane-associated phosphatase activity. Thus, the current rise in segment *b* reflects phosphorylation of a subset of R-domain serines that are highly accessible to phosphatases, and therefore become phosphorylated only at high [PKA] but dephosphorylated instantaneously as soon as [PKA] is lowered (segment *c*). In contrast, the partial channel activity that is reached already at low [PKA] and survives complete PKA removal (segment *d*) is due to a complementary subset of phosphoserines that are little accessible to phosphatases.

Alternatively, *Xenopus* oocyte patch membranes might lack substantial endogenous phosphatase activity. In that case essentially full phosphorylation stoichiometries should be achievable even at low [PKA] (albeit slower; see Fig. 2, green trace), and the currents in segment *d* should reflect those of fully phosphorylated channels since all patches had experienced high [PKA] in segment *b*. But, if indeed phosphorylation is near complete already at relatively low [PKA] (see Fig. 2, *Inset*, dark-blue symbols), then the additional incremental stimulation in high [PKA] (segment *c* versus *d*, Fig. 2, *Inset*, cyan symbols) must reflect reversible stimulation caused simply by PKA binding.

Of note, PKA stocks contain inorganic phosphate (P_i), which itself stimulates CFTR gating (19), but in control experiments the ~5 mM P_i present in solutions of 300 nM PKA enhanced macroscopic currents only by ~20%, which falls short of explaining the observed ~twofold stimulation by 300 nM PKA (*SI Appendix*, Fig. S1).

PKA Strongly, but Reversibly Activates CFTR Channels in the Presence of an ATP Analog Unsuitable for Phosphotransfer. To dissect effects of PKA binding vs. phosphorylation, we sought an ATP analog that gates CFTR but cannot be used by PKA for phosphorylation. N^6-(2-phenylethyl)-ATP (P-ATP) was shown to gate CFTR channels even more potently ($K_{1/2}$ ~ 2 μM) than ATP ($K_{1/2}$ ~ 50 μM) (20, 21). On

the other hand, P-ATP failed to compete off radioactive ATP from PKA, suggesting that it cannot bind to the kinase (22). We therefore tested whether PKA exposure stimulates CFTR currents elicited by P-ATP. When CFTR channels were exposed to 300 nM PKA in the presence of 2 mM ATP (Fig. 3 *A*, *Center*), the tiny current seen before PKA exposure was stimulated ~100-fold, and about half of that maximal current survived PKA removal (Fig. 3*B*, three center bars). For such prephosphorylated channels subsequent exposure to 10 μM P-ATP (Fig. 3 *A*, *Right*) recovered a comparably sized current, although recovery following the prolonged (5-min) exposure to nucleotide-free solution was biphasic, signaling slow recovery of a subset of channels from an inactivated state (23). Importantly, reapplying PKA in P-ATP caused ~twofold further stimulation, which subsided as soon as PKA was removed (Fig. 3*B*, three right bars; the small difference between the two purple bars reflects ongoing slow recovery from the preceding long nucleotide-free period). Moreover, even unphosphorylated channels gating in P-ATP were robustly stimulated by PKA exposure (Fig. 3 *A*, *Left*). This stimulation reflected a robust (~10-fold) acceleration of steady-state single-channel opening rate, coupled with an ~threefold slowing of channel closure (*SI Appendix*, Fig. S2 *A* and *B*), reminiscent of that reported for unphosphorylated channels exposed to PKA + ATP (14). But, whereas in the presence of ATP PKA exposure left a lasting effect which must have reflected phosphorylation (Fig. 3 *B Center*; compare left and right blue bars), in the presence of P-ATP

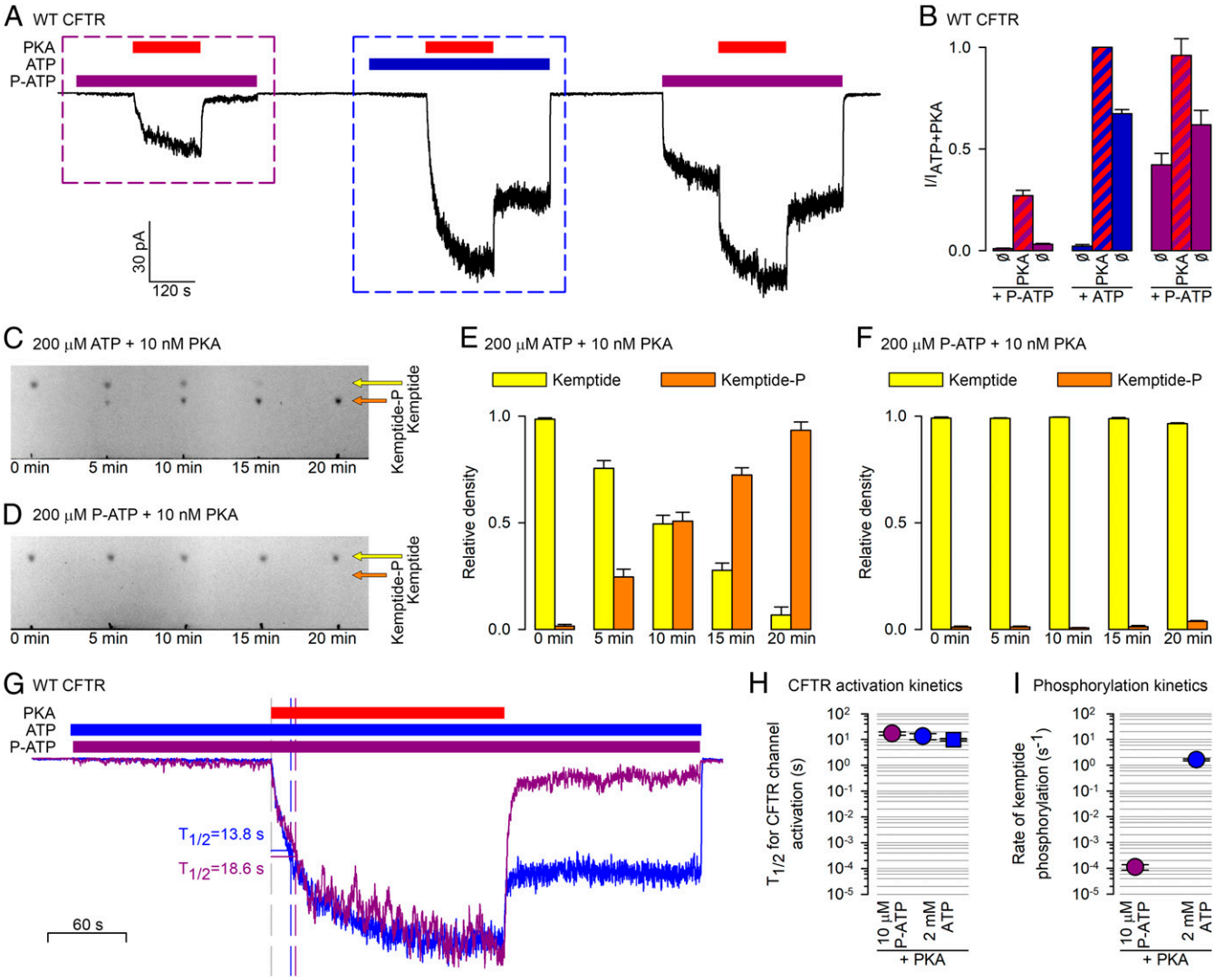

Fig. 3. PKA cannot use P-ATP for phosphotransfer, but reversibly stimulates CFTR channels gating in P-ATP. (*A*) Macroscopic CFTR current in an inside out patch in response to repeated exposures to 300 nM PKA (red bars) in the presence of either 10 μM P-ATP (purple bars) or 2 mM ATP (blue bar). (*B*) Steady-state current amplitudes [mean ± SEM (n = 7–9)], normalized to that observed in ATP + PKA, for the nine segments of the experimental protocol shown in *A*, as indicated below the bars. (*C* and *D*) Kinetics of phosphorylation of TAMRA-kemptide (20 μM) by PKA (10 nM) in the presence of 200 μM ATP (*C*) or P-ATP (*D*), visualized by TLC. Yellow and orange arrows mark the positions of the spots corresponding to the dephospho- and phosphopeptide, respectively. (*E* and *F*) Densitometric analysis of the TLC sheets in *C* and *D*. Relative densities (*Materials and Methods*) of the dephospho- (yellow bars) and phospho-kemptide (orange bars) spots, plotted as a function of incubation time in PKA + ATP (*E*) or PKA+P-ATP (*F*). Bars plot mean ± SEM (n = 3). (*G*) Overlay of the segments of current (purple and blue trace) highlighted by the purple and blue boxes, respectively, in *A*, synchronized to the time points of PKA addition, and renormalized to their respective steady-state amplitudes in PKA. Vertical dashed lines identify the time points at which the currents reach 50% of their steady-state amplitudes ($T_{1/2}$). (*H*) $T_{1/2}$ of current activation for unphosphorylated CFTR channels upon exposure to 300 nM PKA first in 10 μM P-ATP (purple circle) and then in 2 mM ATP (blue circle). As a control, blue square depicts $T_{1/2}$ of activation for channels exposed to 300 nM PKA + 2 mM ATP without prior exposure to PKA+P-ATP (compare Fig. 2, black trace). (*I*) Calculated rates (s^{-1}) of TAMRA-kemptide phosphorylation by PKA in the presence of either 10 μM P-ATP (purple circle) or 2 mM ATP (blue circle). Note logarithmic ordinates in *H* and *I*.

the PKA effect was fully reversible (Fig. 3 *B*, *Left*; compare left and right purple bars).

Of note, the current stimulation by PKA in P-ATP again by far exceeded the marginal effect of 5 mM P_i in P-ATP (*SI Appendix*, Fig. S3), and could also not be explained by a potential contaminant in the P-ATP stock (*SI Appendix*, Fig. S4). Insofar as PKA is indeed unable to use P-ATP for phosphorylation, these results suggest that simple binding of PKA can robustly but reversibly stimulate not only phosphorylated, but even unphosphorylated CFTR channels.

To exclude the possibility that PKA might have used P-ATP for phosphorylation, we next compared rates of phosphorylation in ATP vs. P-ATP of the synthetic PKA substrate TAMRA-kemptide (24). The lower mobility of phospho-kemptide compared to kemptide on TLC sheets (Fig. 3*C*, orange and yellow arrows) allows quantitative estimation of phosphorylation rates by monitoring how the relative densities of the two spots evolve over time (Fig. 3*E*). Using 200 μM ATP, 10 nM PKA, and 20 μM kemptide, ∼50% of the peptide was phosphorylated in 10 min (Fig. 3 *C* and *E*) reporting a k_{cat} of ∼2 s^{-1} (Fig. 3*I*, blue symbol), in good agreement with the earlier report (24). Under the same conditions, but using 200 μM P-ATP, no phosphorylation could be detected in 10 min, and barely any in 20 min (Fig. 3 *D* and *F*). That slow rate of phosphorylation in P-ATP, quantitated by increasing the amount of PKA 250-fold, amounted to ∼1 catalysis per PKA molecule every ∼5 min (*SI Appendix*, Fig. S5 *A* and *B*). Moreover, whereas for ATP the 200 μM concentration was saturating, as expected (*SI Appendix*, Fig. S5 *C* and *D*), for P-ATP raising the concentration fivefold accelerated phosphorylation rate by ∼threefold (*SI Appendix*, Fig. S5 *E* and *F*), suggesting that for P-ATP a 200 μM concentration is still in the quasilinear range. Extrapolating down to the 10 μM P-ATP concentration used in the patch experiments (Fig. 3*A*) the rate of phosphorylation is <1 catalysis per PKA molecule every 2 h (Fig. 3*I*, purple symbol).

Two quantitative arguments firmly exclude the possibility that the current activation observed during the short exposures to PKA in the presence of 10 μM P-ATP (Fig. 3*A*) would have been caused by phosphorylation—even if possibly not just one, but maybe two, three, or a few PKA molecules might be operating simultaneously on the same CFTR channel. First, within ∼1 min of exposure to PKA in P-ATP CFTR current activation was essentially complete, while the probability that any single serine in a CFTR channel might have become phosphorylated during that entire time window is ∼0.007, assuming that the k_{cat} of PKA for the R domain is similar to that for free kemptide in solution. Thus, not more than ∼1% of all CFTR channels in the patch could have been phosphorylated (at a single serine) within that time, whereas the current reached 30–50% of that of a fully phosphorylated channel population (Fig. 3 *A* and *B* and *SI Appendix*, Fig. S3 *A* and *B*). Second, the ratio of phosphorylation rates by PKA in 10 μM P-ATP vs. 2 mM ATP—which is likely independent of the choice of substrate peptide—is ∼1:15,000 (Fig. 3*I*), whereas the kinetics of CFTR channel activation by PKA, quantified as the time required for half-maximal current activation ($T_{1/2}$; Fig. 3*G*), is comparable in P-ATP and ATP (∼10–20 s; Fig. 3*H*). The inevitable conclusion is that PKA robustly activates CFTR channels, either phosphorylated or nonphosphorylated, through simple binding.

PKA Strongly, but Reversibly Activates CFTR Channels that Lack Phosphorylatable Serines. As an alternative approach to test PKA effects on CFTR in the absence of phosphorylation, we generated CFTR constructs in which all PKA-target serines shown to become phosphorylated, including 10 R-domain positions (660, 686, 700, 712, 737, 753, 768, 790, 795, 813) and serine 422 in NBD1 (6–9), were mutated. In one construct (11A-0D) all 11 serines were replaced by alanines, to mimic the dephosphoform. In a second construct (3A-8D) only serine 422 and reportedly "inhibitory" serines 737 and 768 (25, 26) were mutated to alanines, whereas the other eight positions were substituted by aspartates, to assess to what extent stable negative charges mimic phosphorylation.

In earlier studies progressive mutation of an increasing number of R-domain serines progressively diminished channel activation (8, 27–29). Unexpectedly, however, an all-alanine mutant similar to 11A-0D still remained substantially activatable by PKA, reaching a P_o of ∼0.2 (8). This was attributed to phosphorylation of as yet unidentified "cryptic" target serine(s), and much work was invested trying to localize these (8, 27). Consistent with those early studies, in our hands unphosphorylated 11A-0D channels gating in ATP were also robustly stimulated by PKA. Surprisingly, however, most of that activation subsided within seconds of PKA removal (Fig. 4 *A*, *Left*). This contrasts with the behavior of WT CFTR channels (Fig. 4 *E*, *Left*) on which PKA exposure leaves a lasting effect (compare blue bars in Fig. 4 *F*, *Left*). For the 11A-0D mutant the small difference between pre- and post-PKA activities (blue bars in Fig. 4 *B*, *Left*) likely reflects the ongoing slow current recovery after the preceding long nucleotide-free period, a phenomenon also apparent for WT channels (Fig. 4 *E*, *Right*; blue bars in Fig. 4 *F*, *Right*). Importantly, for the 11A-0D mutant a second trial (Fig. 4 *A* and *B*, *Right*) essentially recapitulated the responses seen in the first. Thus, PKA indeed stimulates the 11A-0D mutant but does not cause any lasting effect, making it unlikely that the observed strong activation reflects phosphorylation of some cryptic target serine(s). Rather, the response must reflect PKA binding.

In a previous report, replacement of 4–8 R-domain serines with aspartates was shown to result in channels that can open in ATP without exposure to PKA (28). Indeed, our 3A-8D construct also showed such "constitutive" activity (Fig. 4 *C*, *Left*), but the robust further stimulation of that current by exposure to PKA indicates that the initial, constitutive, P_o must have been very small, all the more so, as even maximal P_o (in PKA + ATP) is expected to be lower for the mutants compared to WT, based on previous studies (8). Thus, in CFTR aspartates are poor mimics of phosphoserines. Importantly, the strong activation of the 3A-8D mutant by PKA was again fully reversible, suggesting that it does not involve phosphorylation (Fig. 4 *C* and *D*). Of note, PKA stimulation of neither mutant could be accounted for by the marginal effect of 5 mM contaminating P_i (*SI Appendix*, Fig. S6).

Discussion

Using an ATP analog that can drive CFTR channel gating but is unsuitable for phosphotransfer by PKA, as well as CFTR channel constructs lacking phosphorylatable serines, we have shown here that both unphosphorylated and phosphorylated CFTR channels are strongly but reversibly activated by simple binding of the protein kinase A catalytic subunit. That conclusion is supported by the four orders of magnitude slower rate of phosphorylation (Fig. 3*I*), but comparable kinetics of CFTR channel activation (Fig. 3 *G* and *H*), by PKA in P-ATP vs. ATP, as well as by the full reversibility of current stimulation by PKA observed for WT CFTR channels in P-ATP (Fig. 3 *A* and *B*) or for phosphorylation-site mutants (Fig. 4 *A*–*D*). Since P-ATP binds poorly to PKA, rapid CFTR channel activation by PKA in P-ATP indicates that the kinase can bind the R domain even in the absence of bound nucleotide, consistent with its established random sequential binding order for ATP and substrate peptides (30–32). On the other hand the slightly (<twofold) slower kinetics of current activation by PKA in P-ATP compared to that in ATP (Fig. 3 *G* and *H*) might be explained by the lack of positive cooperativity between ATP and substrate binding to PKA (33). The reduced fractional stimulation by PKA of 11A-0D compared to WT (10-20-fold vs. 50–100-fold (Fig. 4*B* vs. Fig. 4*F*); ref. 8) suggests that the multiple mutations not only remove the target

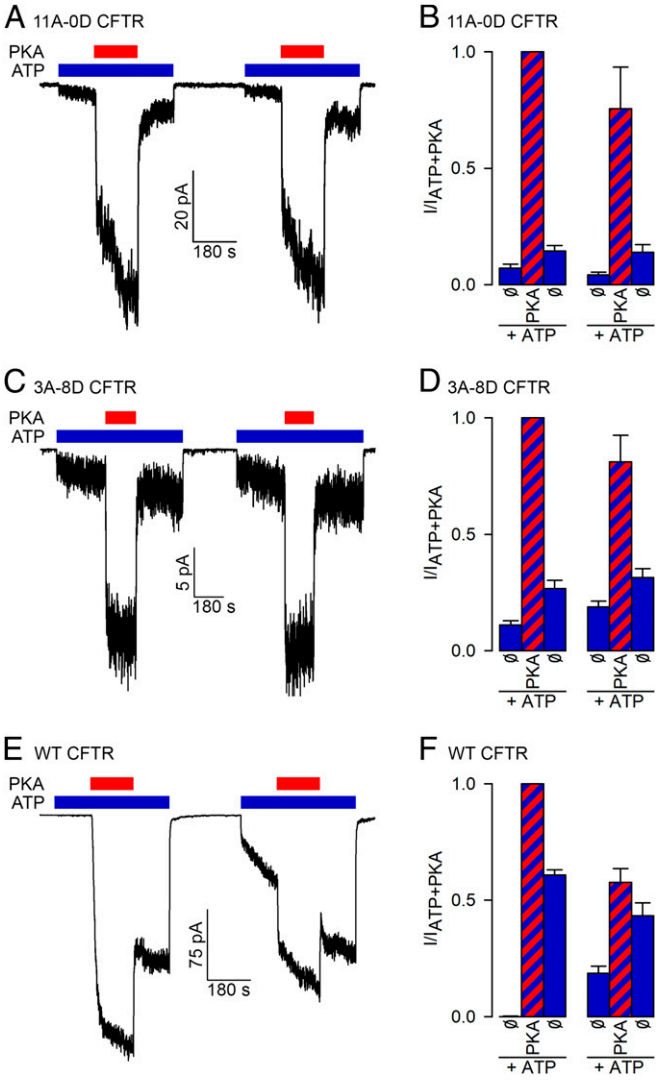

Fig. 4. PKA reversibly stimulates CFTR channels that lack phosphorylatable serines. (*A*, *C*, and *E*) Macroscopic inside out patch currents of (*A*) 11A-0D, (*C*) 3A-8D, and (*E*) WT CFTR channels repeatedly exposed to 300 nM PKA (red bars) in the presence of 2 mM ATP (blue bars). (*B*, *D*, and *F*) Steady-state current amplitudes [mean± SEM (n = 4–11)], normalized to that observed during the first exposure to ATP + PKA, for the six segments of the experimental protocols shown in *A*, *C*, and *E* as indicated below the bars.

serines, but likely also progressively impair PKA binding. Indeed, pseudosubstrate peptides with different substitutions of the target serine display different inhibitory potencies (34), indicating that the identity of the residue at the target position affects binding affinity. Moreover, although disordered, the R domain does contain a significant amount of secondary structure, which is dramatically changed by multiple serine-to-alanine mutations (35). Thus, whether or not reversible stimulation (Fig. 4*A*) reflects PKA binding exclusively to the consensus peptide stretches, it seems reasonable to postulate that its affinity should be reduced in 11A-0D relative to WT.

These findings profoundly reshape our understanding of the mechanism of CFTR activation by PKA (Fig. 5). In the presence of a nucleotide to drive channel gating, even unphosphorylated channels open upon PKA binding (Fig. 3 *A*, *Left*). Insofar as pore opening is unlikely to happen as long as the R domain is in its wedged-in position (13, 14), we infer that PKA binding, without phosphorylation, promotes R-domain release. We suggest (Fig. 5*A*) that there is an equilibrium between intercalated (state 1) and released (state 2) R-domain conformations, which in unphosphorylated channels is strongly shifted toward intercalated. When PKA is present, it can bind the released R domain (state 3), preventing it from returning to the wedged-in position. As long as the R domain is kept outside (states 2 and 3) the channels are "active," in the sense that they can open and close if a suitable nucleoside triphosphate (e.g., ATP or P-ATP) is available. So far, activation is reversible. But, once PKA has also phosphorylated the R domain, the conformational equilibria are irreversibly changed (states 4–6): for the phospho-R domain the equilibrium between wedged-in (state 6) and released (state 5) is shifted toward the released conformation.

Clearly, lumping R-domain phosphorylation at ~10 sites into a single kinetic step is an oversimplification. Correspondingly, the

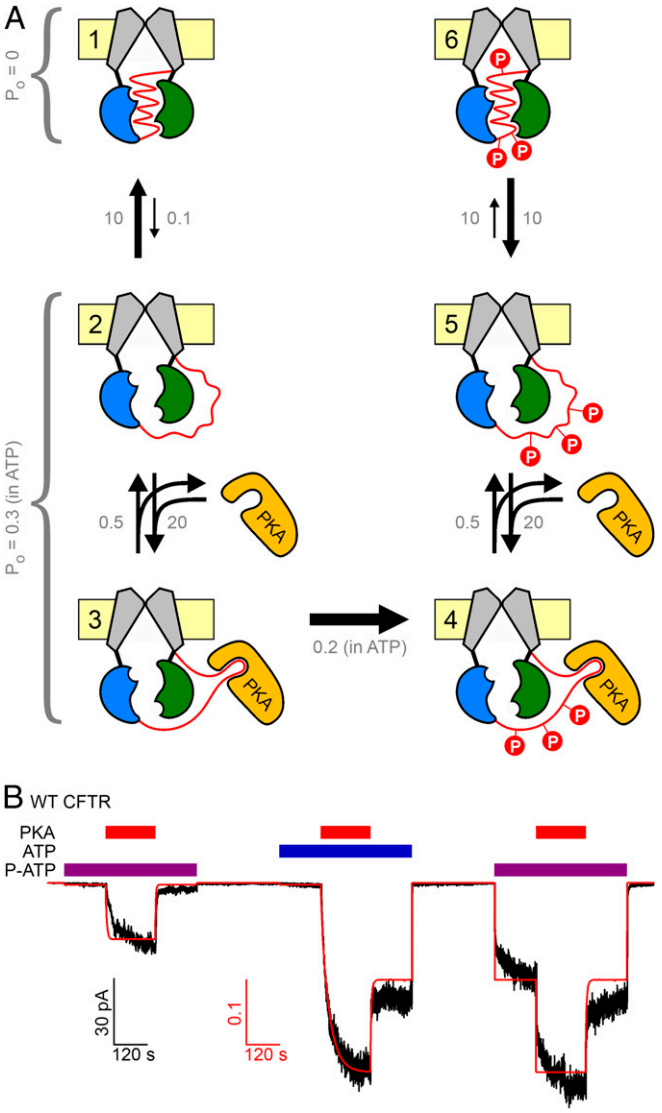

Fig. 5. Mechanistic model of CFTR activation by PKA. (*A*) Simplified equilibrium scheme to describe CFTR activation status using six compound states (numbered). The R domain (red ribbon) is either wedged in (states 1 and 6) or released (states 2–5); the released form can bind PKA (states 3 and 4). In states 4–6 the R domain is phosphorylated (red circles, "P"). States 1 and 6 are inactive (P_o = 0). States 2–5 are active, i.e., they can open and close upon ATP (P-ATP) binding. Domain color coding as in Fig. 1*B*; PKA, orange. (*B*) Experimental current trace (black trace) replotted from Fig. 3*A*, overlaid with calculated open probability time course (red curve) predicted for the same experimental protocol by the scheme in *A*, using the plotted (*gray*) tentative P_o values (in ATP or P-ATP) and rate constants (s^{-1}).

scheme in Fig. 5*A* depicts only two extreme situations: completely unphosphorylated (left column of states) and fully phosphorylated (right column of states). In truth, incremental phosphorylation of the R domain likely incrementally shifts the equilibrium from the wedged-in toward the released form, and fixed negative charges can also do so, albeit much less efficiently (Fig. 4 *C* and *D*). Along those lines, we cannot exclude the possibility that the channels in our patches are already phosphorylated to some extent at the onset of our recordings (e.g., Fig. 3 *A*, *Left*). However, even if so, that basal phosphorylation is clearly insufficient to elicit channel gating, as the estimated P_o (in ATP) is ∼0.003 under such conditions. This argues that the R domain is still in its wedged-in position for most of the time, as depicted for states 1–2 of our simplified model (Fig. 5*A*).

Although this model contains many adjustable parameters, we evaluated how well our data are accounted for by a "minimalist" version, constrained by the following five additional simplifying assumptions. 1) For the state 1 ↔ state 2 equilibrium, we assumed that the unphosphorylated R domain is wedged in for ∼99% of the time ($k_{12}/k_{21} \sim 0.01$), consistent with the tiny pre-PKA current in ATP which is ∼1% of the maximal current in ATP + PKA (Fig. 3 *A*, *Center*). 2) For the state 2 ↔ state 3 equilibrium rate k_{32} is informed by the observed current relaxation rate upon PKA wash-off (∼0.5 s^{-1}; compare Fig. 1*A*), whereas rate k_{23} scales with PKA concentration, shifting the equilibrium toward state 3 at saturating PKA. 3) The lumped rate (k_{34}) of full R-domain phosphorylation was tentatively assigned a value of ∼0.2 s^{-1}, considering a k_{cat} of ∼2 s^{-1} for PKA (Fig. 3 *C* and *E*), but ∼10 target sites to be phosphorylated. 4) Only a single parameter adjustment was made in the right half of the scheme relative to the left: for the phospho-R–domain deocclusion rate (k_{65}) was increased 100-fold, to adjust the equilibrium constant between the wedged-in and released states of the phospho-R domain to $k_{65}/k_{56} \sim 1$. 5) The wedged-in states (states 1 and 6) are inactive ($P_o = 0$), whereas the "released" states (states 2, 3, 4, and 5) are active and might in principle be characterized by distinct P_o values that might further depend on the nucleotide that drives gating (ATP or P-ATP) (18, 20, 21). As a first approximation, we assumed here a single P_o value for all four active states, both in ATP and P-ATP, essentially reducing the model to a binary scheme. Despite evident oversimplification, the macroscopic current time course predicted by this scheme (Fig. 5*A*) for the complex experimental protocol shown in Fig. 3*A* well describes the experimentally observed current amplitudes (Fig. 5*B*, red curve). Obviously, the true picture is far more complex, and further experimental constraints will be required to refine it. But, our simple model provides an initial framework for understanding the molecular mechanism of CFTR channel regulation by its physiological activator, PKA.

In conclusion, we have shown that PKA activates CFTR by binding to the R domain, thereby keeping it away from its "intercalated" position. This finding reveals how an intrinsically disordered peptide segment can serve to regulate protein function through binding to an interacting partner protein. However, in the absence of phosphorylation this type of activation would be immediately reversible upon unbinding of PKA. R-domain phosphorylation therefore serves to leave a lasting footprint, rendering CFTR activation irreversible, undoable only through the action of phosphatases. An intriguing question is how specific the interaction is between the intrinsically disordered R domain and PKA. Indeed, partial CFTR activation through stimulation of Ca^{2+} signaling pathways was also shown to be mediated by direct calmodulin binding to the R domain (36). Given the extended network of proteins that physically and functionally interact with CFTR (37), some of them specifically with the R domain (36, 38), it will be interesting to identify which other proteins might also act as reversible CFTR activators by simply binding the R domain in its released conformation. The potential physiological relevance of such reversible activation, as opposed to irreversible activation by PKA, remains to be established.

Materials and Methods

Molecular Biology. Mutations were introduced (Agilent, QuikChange II) into pGEMHE-CFTR (39). To generate 11A-0D, the codons of amino acid positions 422, 660, 686, 700, 712, 737, 753, 768, 790, 795, and 813 were changed to encode alanines. To generate 3A-8D, the codons of positions 422, 737, and 768 were changed to encode alanines, whereas those of positions 660, 686, 700, 712, 753, 790, 795, and 813 were changed to encode aspartates. Both constructs were confirmed by automated sequencing. Plasmids were linearized (Nhe I, New England Biolabs), transcribed in vitro (mMessage mMachine T7 Kit, Thermo Fisher), and purified RNA stored at −80 °C.

***Xenopus laevis* Oocyte Isolation and Injection.** Oocytes were isolated from anesthetized adult female *Xenopus laevis* following Institutional Animal Care Committee guidelines, injected with 1–10 ng RNA in a fixed 50-nl volume, and stored at 18 °C as described (39). Current recordings were obtained 1–3 d after injection.

Inside Out Patch-Clamp Recording. Patch pipette solution contained (in mM): 136 *N*-Methyl-D-glucamine (NMDG) chloride, 2 $MgCl_2$, 5 Hepes, pH = 7.4 with NMDG. Bath solution contained (in mM): 134 NMDG-Cl, 2 $MgCl_2$, 5 Hepes, 0.5 EGTA, pH = 7.1 with NMDG. MgATP (2 mM) and 2–50 mM P_i (KH_2PO_4) (Sigma-Aldrich) were added from a 400-mM and a 1 M aqueous stock solution, respectively (pH = 7.1 with NMDG). P-ATP (10 μM) was diluted from a 10 mM aqueous stock (Biolog Life Science Institute, purity 99.6%, with 0.4% P-ADP as the only contaminant identifiable by HPLC). The catalytic subunit of bovine PKA (Sigma-Aldrich P2645) was diluted from an ∼18 μM aqueous stock supplemented with 100 μM dithiothreitol (DTT). The continuously flowing bath solution could be exchanged with a time constant of ∼20 ms using electronic valves (ALA-VM8, ALA Scientific Instruments). Experiments were done at 25 °C; membrane potential was −40 mV. Currents were recorded at a bandwidth of 2 kHz (Axopatch 200B, Molecular Devices), digitized at 10 kHz (Digidata 1322A, Molecular Devices), and recorded to disk (pCLAMP 9, Molecular Devices).

Analysis of Current Recordings. Macroscopic CFTR currents were digitally filtered at 50 Hz, downsampled to 100 Hz, and baseline subtracted (pCLAMP 9, Molecular Devices). Mean steady-state currents under various experimental conditions were normalized to that obtained during the first exposure to 2 mM ATP + 300 nM PKA in the same patch. The macroscopic current activation time course in Fig. 1*A* was fit to a two-step activation scheme, W→R→P, yielding sequential activation rates k_{a1} and k_{a2}, and the deactivation time course to a single-step process, P→D, yielding rate k_{PPase}, using nonlinear least-squares methods (pCLAMP 9, Molecular Devices). The time course of channel open probability predicted by the scheme in Fig. 5*A* for the experimental protocol in Fig. 5*B* (Fig. 5*B*, *red curve*) was calculated using standard Q matrix procedures (40).

Determination of Phosphate Concentration. The concentration of contaminant inorganic phosphate (P_i) in our PKA stock solutions was quantified through colorimetric detection of P_i, as described (41). In brief, 150 μL of our standard bath solution supplemented with 3 nM PKA was mixed with 850 μL coloring solution (6:1 vol/vol ratio mixture of 0.42% ammonium molybdate tetrahydrate in 1 N H_2SO_4 and 10% L-ascorbic acid) and incubated for 20 min at 45 °C. Absorption at 820 nm was measured (NanoPhotometer P300, Implen GmbH) and compared to that of a standard curve (1-200 μM KH_2PO_4). All reagents were from Sigma-Aldrich.

Phosphorylation Assay. The reaction buffer contained 50 mM Hepes (pH 7.5), 10 mM Mg-acetate, and freshly added 0.2 mg/mL bovine serum albumine and 5 mM DTT. TAMRA-Kemptide (Addexbio Technologies) was used at a concentration of 20 μM for all experiments. ATP, P-ATP, and PKA were used at various concentrations, as indicated in Fig. 3 and *SI Appendix*, Fig. S5. Reactions were incubated at room temperature (∼23 °C) for 5–20 min. The zero-time control did not contain PKA and was incubated for 20 min. At the end of each incubation a 2-μl aliquot was spotted onto a SIL/UV254 plastic TLC sheet (Macherey-Nagel) and dried in a hot air stream. Once all samples had been loaded, the sheet was developed in a mixture of l-butanol, pyridine, acetic acid, and water (15:10:3:12 vol/vol). The relative densities of the spots corresponding to the dephospho- and phospho-forms of TAMRA-kemptide were quantitated by densitometry (ImageJ). To obtain relative

densities, the total density of each spot, obtained following subtraction of the background, was divided by the sum of the densities of the two spots corresponding to the dephospho- and phospho-forms for that condition.

Statistics. Data are displayed as mean ± SEM, with the number of experiments indicated in the figure legends. For the electrophysiological recordings, *n* represents the number of patches; $n = 5–38$. For the enzymatic activity assays, *n* represents independent technical replicates; $n = 3$. All data were included in the analysis.

Data Availability. Data generated and analyzed over the course of the current study are included within the paper and *SI Appendix*.

ACKNOWLEDGMENTS. This work was supported by Howard Hughes Medical Institute International Early Career Scientist Grant 55007416, EU Horizon 2020 Research and Innovation Program Grant 739593, MTA Lendület Grant LP2017-14/2017, and Cystic Fibrosis Foundation Research Grant CSA-NAD19G0 to L.C., Nemzeti Kutatási, Fejlesztési és Innovációs Hivatal Grant PD 131643 to C.M., and a New National Excellence Program award of the Ministry of Human Capacities of Hungary to Semmelweis University.

1. J. R. Riordan *et al*., Identification of the cystic fibrosis gene: Cloning and characterization of complementary DNA. *Science* **245**, 1066–1073 (1989).
2. C. E. Bear *et al*., Purification and functional reconstitution of the cystic fibrosis transmembrane conductance regulator (CFTR). *Cell* **68**, 809–818 (1992).
3. K. De Boeck, M. D. Amaral, Progress in therapies for cystic fibrosis. *Lancet Respir. Med.* **4**, 662–674 (2016).
4. P. Huang, K. Trotter, R. C. Boucher, S. L. Milgram, M. J. Stutts, PKA holoenzyme is functionally coupled to CFTR by AKAPs. *Am. J. Physiol. Cell Physiol.* **278**, C417–C422 (2000).
5. F. Sun, M. J. Hug, N. A. Bradbury, R. A. Frizzell, Protein kinase A associates with cystic fibrosis transmembrane conductance regulator via an interaction with ezrin. *J. Biol. Chem.* **275**, 14360–14366 (2000).
6. S. H. Cheng *et al*., Phosphorylation of the R domain by cAMP-dependent protein kinase regulates the CFTR chloride channel. *Cell* **66**, 1027–1036 (1991).
7. M. R. Picciotto, J. A. Cohn, G. Bertuzzi, P. Greengard, A. C. Nairn, Phosphorylation of the cystic fibrosis transmembrane conductance regulator. *J. Biol. Chem.* **267**, 12742–12752 (1992).
8. F. S. Seibert *et al*., cAMP-dependent protein kinase-mediated phosphorylation of cystic fibrosis transmembrane conductance regulator residue Ser-753 and its role in channel activation. *J. Biol. Chem.* **270**, 2158–2162 (1995).
9. D. C. Neville *et al*., Evidence for phosphorylation of serine 753 in CFTR using a novel metal-ion affinity resin and matrix-assisted laser desorption mass spectrometry. *Protein Sci.* **6**, 2436–2445 (1997).
10. J. R. Thiagarajah, A. S. Verkman, CFTR pharmacology and its role in intestinal fluid secretion. *Curr. Opin. Pharmacol.* **3**, 594–599 (2003).
11. L. S. Ostedgaard, O. Baldursson, D. W. Vermeer, M. J. Welsh, A. D. Robertson, A functional R domain from cystic fibrosis transmembrane conductance regulator is predominantly unstructured in solution. *Proc. Natl. Acad. Sci. U.S.A.* **97**, 5657–5662 (2000).
12. P. Vergani, S. W. Lockless, A. C. Nairn, D. C. Gadsby, CFTR channel opening by ATP-driven tight dimerization of its nucleotide-binding domains. *Nature* **433**, 876–880 (2005).
13. Z. Zhang, J. Chen, Atomic structure of the cystic fibrosis transmembrane conductance regulator. *Cell* **167**, 1586–1597.e9 (2016).
14. F. Liu, Z. Zhang, L. Csanády, D. C. Gadsby, J. Chen, Molecular structure of the human CFTR Ion Channel. *Cell* **169**, 85–95.e8 (2017).
15. Z. Zhang, F. Liu, J. Chen, Conformational changes of CFTR upon phosphorylation and ATP binding. *Cell* **170**, 483–491.e8 (2017).
16. Z. Zhang, F. Liu, J. Chen, Molecular structure of the ATP-bound, phosphorylated human CFTR. *Proc. Natl. Acad. Sci. U.S.A.* **115**, 12757–12762 (2018).
17. D. P. Rich *et al*., Effect of deleting the R domain on CFTR-generated chloride channels. *Science* **253**, 205–207 (1991).
18. L. Csanády *et al*., Severed channels probe regulation of gating of cystic fibrosis transmembrane conductance regulator by its cytoplasmic domains. *J. Gen. Physiol.* **116**, 477–500 (2000).
19. M. R. Carson, S. M. Travis, M. C. Winter, D. N. Sheppard, M. J. Welsh, Phosphate stimulates CFTR Cl- channels. *Biophys. J.* **67**, 1867–1875 (1994).
20. Z. Zhou *et al*., High affinity ATP/ADP analogues as new tools for studying CFTR gating. *J. Physiol.* **569**, 447–457 (2005).
21. L. Csanády, C. Mihályi, A. Szollosi, B. Töröcsik, P. Vergani, Conformational changes in the catalytically inactive nucleotide-binding site of CFTR. *J. Gen. Physiol.* **142**, 61–73 (2013).
22. S. Schauble *et al*., Identification of ChChd3 as a novel substrate of the cAMP-dependent protein kinase (PKA) using an analog-sensitive catalytic subunit. *J. Biol. Chem.* **282**, 14952–14959 (2007).
23. M. F. Tsai, M. Li, T. C. Hwang, Stable ATP binding mediated by a partial NBD dimer of the CFTR chloride channel. *J. Gen. Physiol.* **135**, 399–414 (2010).
24. K. Viht, A. Vaasa, G. Raidaru, E. Enkvist, A. Uri, Fluorometric TLC assay for evaluation of protein kinase inhibitors. *Anal. Biochem.* **340**, 165–170 (2005).
25. D. J. Wilkinson *et al*., CFTR activation: Additive effects of stimulatory and inhibitory phosphorylation sites in the R domain. *Am. J. Physiol.* **273**, L127–L133 (1997).
26. L. Csanády *et al*., Preferential phosphorylation of R-domain Serine 768 dampens activation of CFTR channels by PKA. *J. Gen. Physiol.* **125**, 171–186 (2005).
27. X. B. Chang *et al*., Protein kinase A (PKA) still activates CFTR chloride channel after mutagenesis of all 10 PKA consensus phosphorylation sites. *J. Biol. Chem.* **268**, 11304–11311 (1993).
28. D. P. Rich *et al*., Regulation of the cystic fibrosis transmembrane conductance regulator Cl- channel by negative charge in the R domain. *J. Biol. Chem.* **268**, 20259–20267 (1993).
29. C. J. Mathews *et al*., Dibasic protein kinase A sites regulate bursting rate and nucleotide sensitivity of the cystic fibrosis transmembrane conductance regulator chloride channel. *J. Physiol.* **508**, 365–377 (1998).
30. C. T. Kong, P. F. Cook, Isotope partitioning in the adenosine 3′,5′-monophosphate dependent protein kinase reaction indicates a steady-state random kinetic mechanism. *Biochemistry* **27**, 4795–4799 (1988).
31. J. A. Adams, Kinetic and catalytic mechanisms of protein kinases. *Chem. Rev.* **101**, 2271–2290 (2001).
32. S. S. Taylor *et al*., PKA: A portrait of protein kinase dynamics. *Biochim. Biophys. Acta* **1697**, 259–269 (2004).
33. L. R. Masterson, A. Cembran, L. Shi, G. Veglia, Allostery and binding cooperativity of the catalytic subunit of protein kinase A by NMR spectroscopy and molecular dynamics simulations. *Adv. Protein Chem. Struct. Biol.* **87**, 363–389 (2012).
34. J. R. Feramisco, E. G. Krebs, Inhibition of cyclic AMP-dependent protein kinase by analogues of a synthetic peptide substrate. *J. Biol. Chem.* **253**, 8968–8971 (1978).
35. A. M. Dulhanty, X. B. Chang, J. R. Riordan, Mutation of potential phosphorylation sites in the recombinant R domain of the cystic fibrosis transmembrane conductance regulator has significant effects on domain conformation. *Biochem. Biophys. Res. Commun.* **206**, 207–214 (1995).
36. Z. Bozoky *et al*., Synergy of cAMP and calcium signaling pathways in CFTR regulation. *Proc. Natl. Acad. Sci. U.S.A.* **114**, E2086–E2095 (2017).
37. S. Pankow *et al*., ΔF508 CFTR interactome remodelling promotes rescue of cystic fibrosis. *Nature* **528**, 510–516 (2015).
38. S. B. Ko *et al*., Gating of CFTR by the STAS domain of SLC26 transporters. *Nat. Cell Biol.* **6**, 343–350 (2004).
39. K. W. Chan, L. Csanády, D. Seto-Young, A. C. Nairn, D. C. Gadsby, Severed molecules functionally define the boundaries of the cystic fibrosis transmembrane conductance regulator's NH(2)-terminal nucleotide binding domain. *J. Gen. Physiol.* **116**, 163–180 (2000).
40. D. Colquhoun, F. J. Sigworth, "The principles of the stochastic interpretation of ion-channel mechanisms" in *Single Channel Recording*, B. Sakmann, E. Neher, Eds. (Plenum Press, New York, 2nd Ed., 1995), pp. 397–482.
41. I. Iordanov, B. Tóth, A. Szollosi, L. Csanády, Enzyme activity and selectivity filter stability of ancient TRPM2 channels were simultaneously lost in early vertebrates. *eLife* **8**, e44556 (2019).